arXiv:1210.1574v1 [astro-ph.CO] 4 Oct 2012

Detection of a virial shock around the Coma galaxy cluster

Uri Keshet,[1,*] Doron Kushnir,[2] Abraham Loeb,[3] and Eli Waxman[4]

[1] *Physics Department, Ben-Gurion University of the Negev, POB 653, Be'er-Sheva 84105, Israel*
[2] *Institute for Advanced Study, Einstein Drive, Princeton, New Jersey 08540, USA*
[3] *Harvard-Smithsonian Center for Astrophysics, 60 Garden St., Cambridge, MA 02138, USA*
[4] *Physics Faculty, Weizmann Institute of Science, POB 26, Rehovot, Israel*

Galaxy clusters, the largest gravitationally bound objects in the Universe, are thought to grow by accreting mass from their surroundings through large-scale virial shocks. Due to electron acceleration in such a shock, it should appear as a γ-ray, hard X-ray, and radio ring, elongated towards the large-scale filaments feeding the cluster, coincident with a cutoff in the thermal Sunyaev-Zel'dovich (SZ) signal. However, no such signature was found so far, and the very existence of cluster virial shocks has remained a theory. We report the discovery of a large, ~ 5 Mpc diameter γ-ray ring around the Coma cluster, elongated towards the large scale filament connecting Coma and Abell 1367. The γ-ray ring correlates both with a synchrotron signal and with the SZ cutoff. The γ-ray, hard-X-ray, and radio signatures agree with analytic and numerical predictions, if the shock deposits a few percent of the thermal energy in relativistic electrons over a Hubble time, and $\sim 1\%$ of the energy in magnetic fields. The implied inverse-Compton and synchrotron cumulative emission from similar shocks dominates the diffuse extragalactic γ-ray and low frequency radio backgrounds. Our results reveal the prolate structure of the hot gas in Coma, the feeding pattern of the cluster, and properties of the surrounding large scale voids and filaments. The anticipated detection of such shocks around other clusters would provide a powerful new cosmological probe.

1. INTRODUCTION AND OVERVIEW

In the hierarchical paradigm of large scale structure (LSS) formation, galaxy clusters are the largest object ever to virialize. With masses in excess of $10^{14} M_{\odot}$, they are located at the nodes of the cosmic web, where they accrete matter from the surrounding voids and through large scale filaments. Due to their vast size, galaxy clusters resemble island Universes seen at great distance, providing a powerful cosmological probe and a unique astrophysical laboratory.

The gas accreted by a cluster is thought to abruptly heat and slow down in a strong virial shock wave surrounding the cluster. Such collisionless shocks are thought, by analogy with supernova remnant shocks, to accelerate charged particles to $>$ TeV energies, where they Compton-scatter cosmic-microwave background (CMB) photons up to the γ-ray band[1–3]. Consequently, one expects to find γ-ray rings around clusters[4], as indicated by cosmological simulations[3,5], which suggest an elliptic morphology elongated towards the large-scale filaments feeding the cluster[3]. Such rings are also expected in hard X-rays[6], and should coincide with a synchrotron radio ring[4,7] and with a cutoff in the thermal Sunyaev-Zel'dovich (SZ) signal[8].

However, no such virial shock signature was detected so far, although a stacking analysis of EGRET data around a sample of 447 rich clusters did show a 3σ signal[9]. Upper limit were imposed on the γ-ray emission from clusters such as Coma[10–13], but mostly focusing on the central parts of the cluster, well within the virial radius. The very existence of cluster-scale virial shocks has thus remained unconfirmed.

The Coma cluster (Abell 1656) is one of the richest nearby clusters. With mass $M \sim 10^{15} M_{\odot}$, temperature $T \sim 8$ keV, and richness class 2, it lies only ~ 100 Mpc away[14], at a redshift $z = 0.023$. Its virial radius, $R \simeq R_{200} \simeq 2.3$ Mpc, corresponds to an angular radius $\psi \simeq \psi_{200} \simeq 1.3°$, where subscript 200 refers to an enclosed density 200 times above the critical value. The cluster is somewhat elongated in the East-West direction, in coincidence with the Western LSS filament[15] that connects it with the cluster Abell 1367 (see Figure 6a). There is X-ray, optical, weak lensing, radio[16], and SZ[17] evidence that the cluster is accreting clumpy matter and experiencing weak shocks towards the filament well within the virial radius, at $\psi \sim 0.5°$ radii.

The VERITAS Čerenkov array has produced a $d \sim 5°$ diameter γ-ray mosaic[13] of Coma, at energies $E \gtrsim 220$ GeV. We argue that the significance map (Figure 1a) shows extended γ-ray emission away from the center, that appears as a thick ($\sim 0.5°$) elliptical ring with semi-minor axis $b \simeq 1.3°$, elongated along the East–West direction, with semi-major to semi-minor axes ratio $\zeta = a/b \gtrsim 3$. The ring is seen at a 4.5σ confidence level (effectively a single-parameter fit, estimated using mock VERITAS noise maps; see Figures 2 and 3 and §2). However, the data was taken in $\mathsf{w} = 0.5°$ wobble mode[18], inappropriate for extended emission on larger scales; correcting for the excessive background removal indicates a $\geq 5.7\sigma$ signal.

X-ray and galaxy maps suggest that the LSS filament and the semi-major axis of the thermal gas distribution are slightly tilted Southwest, at an angle $-10° \lesssim \phi \lesssim 0°$. Indeed, the significance of the γ-ray structure is maximized when thus tilted; the best fit is obtained for $\zeta \simeq 4.5$ and $\phi \simeq -5°$. If no assumption is made regarding ϕ, the

---

[*] ukeshet@bgu.ac.il

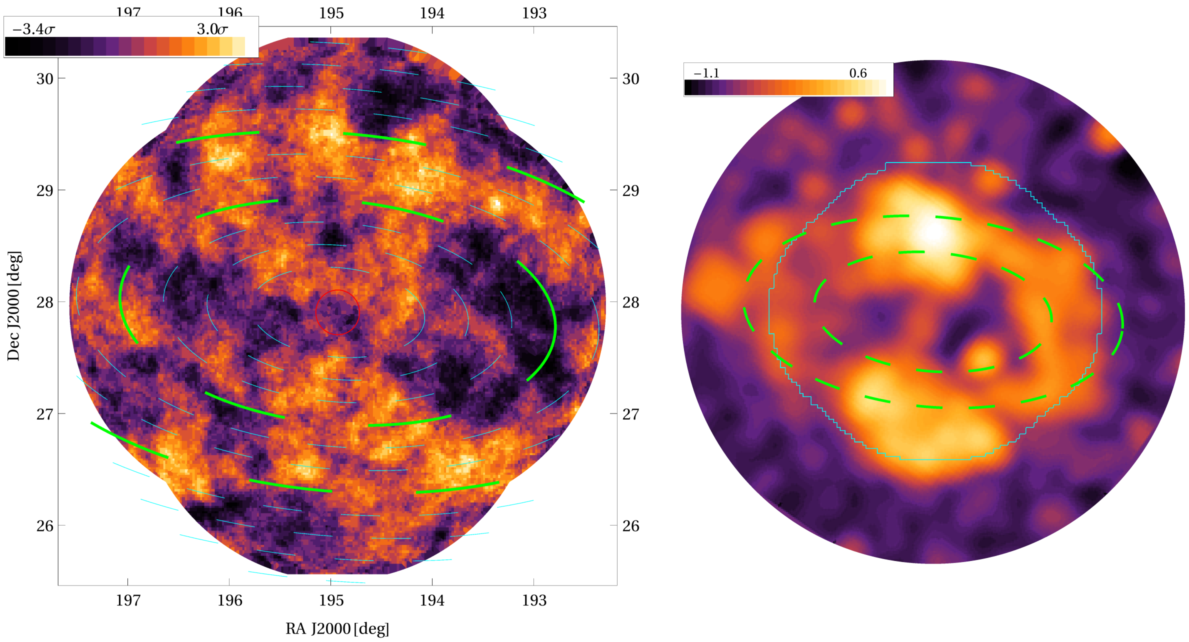

(a) VERITAS significance map

(b) Simulated cluster in γ-rays

FIG. 1: **Observed and simulated γ-ray maps of Coma.**
Left: VERITAS $\gtrsim 220$ GeV significance map[13] of Coma for $\theta = 0.2°$ integration (illustrated by the red circle). Elliptical bins are shown (thin dashed cyan contours) for $\Delta b = 0.2°$, $\zeta = a/b = 2$ and $\phi = -5°$. The bins showing enhanced emission are highlighted (bounded by thick, long-dashed green curves). *Right:* Simulated map of a Coma-like cluster from a ΛCDM simulation[3]. The largest in the 200 Mpc simulation box, this cluster has[7] mass $M \simeq 10^{15} M_\odot$ and temperature $T \simeq 8$ keV. The 8.5° diameter image was convolved with a $\sim 0.23°$ beam, comparable to the VERITAS map, and rotated such that the large-scale filament extends to the West. Colorbar: $\log_{10}(J/10^{-8}\ \mathrm{cm}^{-2}\ \mathrm{s}^{-1}\ \mathrm{ster}^{-1})$ brightness above 220 GeV for $\dot{u}\xi_e = 5\%$. The regions corresponding to the VERITAS mosaic (solid cyan contour) and to the VERITAS ring (elliptic dashed contours) are highlighted.

ring significance weakens to 4.2σ ($\geq 5.4\sigma$ corrected).

The size and morphology of the VERITAS ring resemble the predicted γ-ray signature of a Coma-like, $M \sim 10^{15} M_\odot$ and $T \sim 8$ keV cluster in a ΛCDM simulation[3]. The simulated map (Figure 1b), oriented such that the major simulated LSS filament lies to the West and normalized for a nominal 3.3σ wobble-mode VERITAS detection (no remaining free parameters), correlates with the VERITAS map at the 3.7σ (4.9σ corrected) confidence level.

The ring brightness agrees with predictions too, if the relativistic electron fraction ξ_e of the thermal energy accretion rate $\dot{u}$ (normalized by the total thermal energy over a Hubble time) is a few percent. The associated $\sim 5\ \mathrm{eV\ s^{-1}\ cm^{-2}}$ flux at 20–80 keV energies can explain the hard X-ray signal observed in Coma[19]. Similar, $\xi_e \dot{u} \simeq 4\%$ values are inferred from the 3σ EGRET stacking analysis[9], and from LSS hard X-ray sources[6,20].

In order to examine the coincident radio signals, we spectrally decompose the WMAP seven-year, full-sky maps[21] into synchrotron and thermal SZ maps. Excluding the inner, $b < 1°$ part of the cluster, the VERITAS data correlates with the synchrotron map at a $+2.8\sigma$ ($+3.9\sigma$) confidence level (Figure 9), and anti-correlates with the SZ signal at -2.6σ (-3.6σ). The radio signals are stronger in the Western half of the ring, towards the LSS filament, where the correlations strengthen up to $+3.5\sigma$ ($+4.6\sigma$) with the synchrotron and -3.9σ (-5.0σ) with the SZ.

These peripheral radio signals agree with predictions for the synchrotron emission from the γ-ray emitting electrons, and for the SZ decline with thermal pressure beyond the shock, provided that $B \simeq 0.6\ \mu$G magnetic fields are found downstream, corresponding to $\xi_B \simeq 1\%$ magnetization. Bright spots along the ring suggest local enhancements, up to $\dot{u}\xi_e\xi_B \sim$ a few times its mean value.

While the SZ signal, extending in some parts out to $\psi \simeq 2.3°$, agrees with SZ detections by WMAP[21] and Planck[17], the peripheral synchrotron signal coincident with the γ-rays and with the SZ cutoff was not reported so far. Note that the γ-ray ring and these radio features are much farther out than the $\psi \simeq 0.5°$ weak shocks previously reported based on X-ray, radio[16], and SZ[17] data.

Inside the $b = 1°$ ellipse, the VERITAS and synchrotron maps show a -1.9σ (-2.7σ) anti-correlation, mainly (-2.2σ (-2.8σ)) in the West, evident from the γ-ray underluminous radio halo and relic (Figure 9). Such a signature, predicted in secondary models[22] where cosmic-

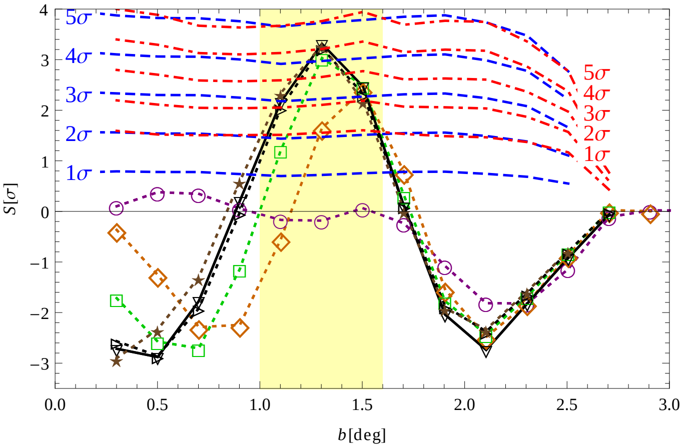

FIG. 2: **Significance of the VERITAS ring.** Elliptical binning (symbols; connecting lines are guides to the eye) of the significance map (Figure 1a) with $\Delta b = 0.6°$, an East-West orientation ($\phi = 0$), and semi-major to semi-minor axes ratios $\zeta \equiv a/b = 1$ (circles), 2 (diamonds), 3 (squares), 5 (right triangles) and 1000 (stars). A slightly tilted, $\phi = -5°$ orientation provides a slightly better fit, illustrated for $\zeta = 5$ (down triangles and solid line). The yellow band corresponds to the bright extended ring marked in Figure 1a. The detection significance of the ring can be estimated from the enclosed flux (the ordinate gives the nominal significance S), but more accurate estimates are found by considering a large sample of mock maps containing only noise, and applying the same elliptical templates, either constrained to have an East-West elongation (labelled dashed lines) or picking the angle ϕ that maximizes the significance in each map (labelled dot-dashed lines). In either case, a correction due to excessive wobble-mode background subtraction is necessary.

ray ion collisions inject relativistic electrons in both strongly ($\gtrsim 3\ \mu$G) and weakly magnetized regions, which consequently appear radio bright/γ-ray faint and vice versa, is unnatural in primary models where electrons are (re)accelerated in turbulence[23,24] or weak shocks. Secondary electrons can explain radio halos[25,26], relics[22] and minihalos[27] as arising from the same cosmic-ray distribution, if the latter is nearly homogeneous[22]. The extent and magnitude of the anti-correlation observed, if confirmed, support such secondary models, and favor an extended cosmic-ray distribution.

A future VERITAS observation deeper than the present 18.6 hour exposure would decisively test our results, in particular if wobble-mode corrections are minimized. This would allow a more precise reconstruction of the virial shock and a measure of variations in the electron deposition rate along the shock front. Such data is valuable in the study of LSS formation at low redshifts, mapping the feeding pattern of Coma, probing the surrounding voids and filaments, and tracing the warm-hot intergalactic medium (WHIM) immediately behind the shock.

A detailed, more significant anti-correlation between γ-ray and synchrotron maps at inner, $\psi \lesssim 1°$ radii would confirm the hadronic, secondary electron model for cluster radio sources, and provide a direct measure of magnetic variations in the ICM. A deeper γ-ray observation would thus probe the cosmic-ray proton distribution out to large radii, address the origin of these protons, and place an upper limit on proton acceleration in the virial shock.

The VERITAS energy threshold, $E \simeq 220$ GeV, is not far below the expected photon cutoff, $E_{max} \simeq 50(B/0.6\ \mu\text{G})$ TeV. Observations at higher energies would become increasingly sensitive to this cutoff, thus probing the conditions at the shock. Interestingly, no evidence for extended emission was found in a 1.1 TeV observation of Coma by the HESS telescopes[28], with $\sim 40\%$ the sensitivity in the VERITAS mosaic, but the γ-ray ring may be shallowly buried in the HESS noise.

Calibrating analytic[1,3], and numerical[3,7] estimates with the above $\dot{u}\xi_e$ and ξ_B values, yields $E^2 dJ/dE \simeq 0.3\ \text{keV}(\xi_e \dot{u}/5\%)\ \text{s}^{-1}\ \text{cm}^{-2}\ \text{ster}^{-1}$ inverse-Compton and $\nu I_\nu \sim 3 \times 10^{-11}(\xi_e \dot{u}/5\%)(\xi_B/1\%)\ \text{erg s}^{-1}\ \text{cm}^{-2}\ \text{ster}^{-1}$ synchrotron cumulative backgrounds from cluster shocks. These constitute fair fractions of the γ-ray and low-frequency radio signals observed far from the Galactic plane, and dominate the respective diffuse extragalactic backgrounds[7,29].

The paper is organized as follows. In §2 we show that an elongated γ-ray ring around Coma was observed by the VERITAS Čerenkov array. Methods to correct for excessive wobble-mode background subtraction are discussed in general in §3, and specifically for cross-correlation analyses in §4. Contamination by Galactic foregrounds is shown to be negligible in §5. The γ-ray ring is shown to agree with simulation-based predictions in §6. Significant correlations with both synchrotron and SZ maps are presented in §7. In §8 we show that the γ-ray signal agrees with predictions, if the shock deposits a few percent of the thermal energy per Hubble time in relativistic electrons. In §9 we show that the synchrotron and SZ signals also agree with the predictions, if magnetic fields carry $\xi_B \simeq 1\%$ of the thermal energy. A γ-ray–radio anti-correlation inward of the γ-ray ring is interpreted in §10 as possible preliminary evidence for strong local magnetization and secondary electron injection at small radii. The results are summarized and discussed in §11. A simple β-model of the shock is provided in Appendix A.

We adopt a concordance flat ΛCDM model with hubble constant $H = 70$ km Mpc^{-1}, a baryon fraction $f_b = 17\%$, and a hydrogen mass fraction $\chi = 0.75$. The plasma is approximated as an ideal gas with adiabatic index $\Gamma = 5/3$ and mean particle mass $\mu = 0.59 m_p$, where m_p is the proton mass. Colorbars are square-weighted.

2. VERITAS γ-RAY RING AROUND COMA

VERITAS has produced a $d \sim 5^\circ$ diameter γ-ray mosaic[13] of Coma, at energies $\gtrsim 220$ GeV. The significance map (Figure 1a), taken in $\mathsf{w} = 0.5^\circ$ wobble mode[18] with a $\theta = 0.2^\circ$ integration radius, shows some extended γ-ray emission away from the center. The γ-ray structure appears as an elliptical ring, elongated along the East-West direction, or as two parallel filaments lying symmetrically both North and South of the cluster. The spectrum in the VERITAS band is probably flat, as a $p = 2.4$ photon spectral index was used to optimize the gamma-hadron separation cuts[13]. In §8 we show that a flat spectrum with index $p = 2$ (equal energy per logarithmic energy interval) is consistent with observations at lower energies.

Denote the VERITAS significance map by s_j. The data is taken in wobble mode[18], where a pixel of significance s_j means that in a beam of radius $\theta = 0.2^\circ$ centered upon the pixel, there are $s_j N_\sigma$ counts in excess of the anticipated $N_{0.2}$ background events, where $N_\sigma \equiv N_{0.2}^{1/2}$ and the background is estimated based on a $\mathsf{w} \sim 0.5^\circ$ ring around the pixel. A θ^2 analysis[13] shows a background of about $N_{0.2} \simeq 1000$ photon counts above 220 GeV in such a $\theta = 0.2^\circ$ bin. The background per pixel is denoted by $N_b = N_{0.2}/\mathsf{n}_{0.2}$, where $\mathsf{n}_{0.2}$ is the number of pixels in the beam. First we assume that the background is uniform, so the pixels are not correlated before the beam integration. The nominal significance of an extended source may then be estimated as

$$S = \frac{s N_\sigma/\mathsf{n}_{0.2}}{\sqrt{N_b \mathsf{n}}} = \frac{s}{\sqrt{\mathsf{n}_{0.2}\mathsf{n}}} \ , \tag{1}$$

where $s = \sum s_j$ and n are respectively the total significance and the number of pixels enclosed.

In order to quantify the γ-ray structure and assess its significance, we fit the data with a thick, elliptical ring model. The center of the ellipse is chosen as the ROSAT X-ray peak. The median semi-major axis a is taken along the East-West direction, as inferred from the ROSAT map and from the orientation of the SDSS galaxy filament. The thickness of the ring is fixed at $\Delta b = 0.6^\circ$ along the semi-minor axis, because a thicker ring would exceed the $2\mathsf{w} = 1^\circ$ limit imposed by the wobble-mode background subtraction[30]. The ring is then defined by its median semi-minor axis b and elongation ratio $\zeta = a/b$, taken as two free parameters. However, for sufficient elongation, $\zeta \gtrsim 3$, the results (Figures 2 and 3) depend weakly upon ζ. The (effectively single-parameter) fit then indicates an extended structure around $b \simeq 1.3^\circ$, found at an $S = 3.3\sigma$ nominal significance level.

The SDSS (Figure 6a) and ROSAT maps suggest that the LSS filament and the semi-major axis of the gas distribution are slightly tilted towards the Southwest, at an angle $-10^\circ \lesssim \phi \lesssim 0^\circ$. Indeed, the significance of the γ-ray structure is maximized when tilted at precisely such angles (Figure 3). The best fit is obtained for $\zeta \simeq 4.5$ and $\phi \simeq -5^\circ$.

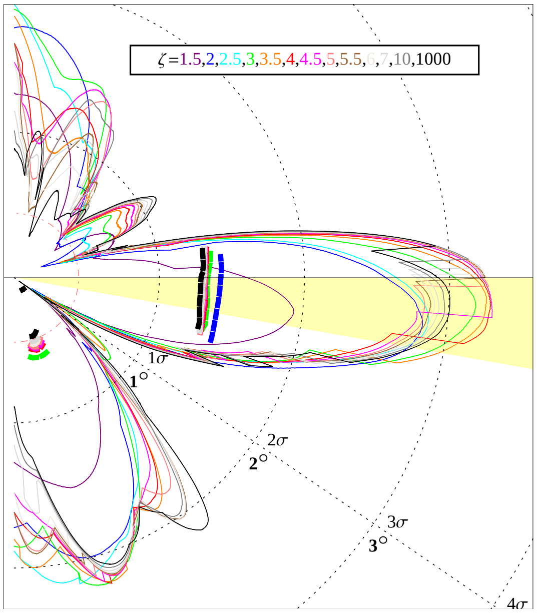

FIG. 3: **Orientation of the VERITAS ring.** The nominal significance S (thin, solid curves) and corresponding semi-minor axes b (thick, dashed curves) are shown for elongated rings of various ellipticity ζ (legend). The yellow sector corresponds to the $-10^\circ < \phi < 0^\circ$ orientation of the LSS filament. The secondary peak towards $\phi \simeq 70^\circ$ with $b \sim 0.5^\circ$ is related to the primary peak: the semi-major axis of the small ellipse solution roughly coincides with the semi-minor axis of the large ellipse solution.

A more reliable way to estimate the significance of the extended emission is to apply the same elliptical templates to a large sample (~ 1000) of mock significance maps, containing random noise but no signal. We prepare these maps by injecting Poisson noise at the observed background level to the VERITAS mosaic template, integrating over the same $\theta = 0.2^\circ$ beam, and converting to a significance map using either the mean background or a simulated $\mathsf{w} = 0.5^\circ$ wobble-mode background.

None of the resulting mock maps shows a signal as strong as the observed $S = 3.3\sigma$, so we extrapolate to the high significance levels assuming a Gaussian distribution. The resulting significance levels are shown as dashed curves in Figure 2, for elliptical rings elongated in the East-West direction (based on 1000 maps at a given ζ). If we make no a-priori assumption regarding the ring orientation ϕ, but rather choose in each mock map the value ϕ that maximizes its nominal ring significance, we obtain higher mock detection levels, shown as dot-dashed contours in the figure (based on 200 maps, each scanned with $\Delta\phi = 20^\circ$ tilt intervals). The results depend weakly (within the statistical fluctuations) on ζ.

The mock statistics indicate that the VERITAS ring presents at the 4.5σ confidence level if we assume that it is aligned with the LSS filament, and at 4.2σ confidence if we make no a-priori assumption regarding ϕ. These conservative estimates are based on the mean background, and are approximately independent of ζ; higher, $\sim 5.5\sigma$ significance levels are obtained when wobble-mode is used to estimate the mock background. As we show in §3 below, the detection significance for such extended structures is actually higher, $\geq 5.7\sigma$ for East-West alignment, and ≥ 5.4 for arbitrary ϕ.

The signal is locally on the order of $\lesssim 10\%$ of the noise, and stronger than the average Galactic foreground at these energies[31] (see §8). In the Coma region, the expected Galactic foreground is relatively low, spatially smooth, and featureless on $\lesssim 0.5°$ scales; see §5. Wobble-background subtraction is highly efficient in removing smooth foregrounds; a disadvantage is that it also removes much of the signal for extended sources.

In wobble mode, an estimated background is subtracted based on a ring of radius w around each pixel. This method, appropriate for point sources, distorts and smears out features extended over scales comparable or larger than w. As we show below, analyses of the γ-ray features, of a histogram of the γ-ray pixels, and of wobble simulations, indicate that the wobble subtraction reduces the significance of the extended features observed by at least $\Delta S = 1.2\sigma$. Therefore, the corrected significance of a γ-ray ring aligned with the LSS filament is estimated as $\geq 5.7\sigma$.

3. CORRECTING FOR WOBBLE-MODE BACKGROUND SUBTRACTION

Consider the wobble-induced correlation between γ-ray pixels. Due to the wobble background subtraction, the significance of a pixel is anti-correlated with the pixels $\mathsf{w} \sim 0.5°$ around it. One implication is that sources that extend over scales much larger than w are effectively erased by the background subtraction, except in an $\sim \mathsf{w}$ wide band in their periphery. In such a band, and in sources that extend $\lesssim \mathsf{w}$ in at least one direction, the signal is diminished but not completely erased. For example, the estimated signal at the inner edge of a large linear source will be diminished by a factor of two, and the signal at the outer edge will have an equal but negative significance. Therefore, for sources that extend over $> \mathsf{w}$ in at least one direction, the actual significance may be $\gtrsim 2$ times higher than estimated from the wobble-mode map.

In order to quantify the effect wobble-mode has on the signal, we examine the distribution of γ-ray significance pixels, using the same $\theta = 0.2°$ integration beam applied to the map. The significance histogram (Figure 4), taken with $\delta\sigma = 0.1$ intervals, can be modeled[13] as a single Gaussian function, with adjusted coefficient of determination $\bar{R}^2 = 0.9956$.

However, the histogram shows peak deviations and sharp cutoffs, indicating a more complicated underlying distribution. Indeed, a simple model combining two Gaussian functions provides a much better fit to the data ($\bar{R}^2 = 0.9967$; note that $\bar{R}$ improves slowly near 1). The best fit is obtained for Gaussian means $\mu_1 = -1.23 \pm 0.21$ and $\mu_2 = 0.23 \pm 0.15$, with corresponding standard deviations 0.69 ± 0.12 and 0.91 ± 0.08. The data were also modelled as the sum of two Gaussian functions constrained to have the same standard deviation; the resulting best fit is similar to the unconstrained sum: $\mu_1 = -0.96 \pm 0.06$ and $\mu_2 = 0.41 \pm 0.05$, with standard deviation 0.83 ± 0.04 ($\bar{R}^2 = 0.9967$).

Both fits suggest that a signal is present in the map, with pixels that are on average $\mu_2 - \mu_1 \simeq 1.4\sigma$ above the noise. Interestingly, a histogram of the pixels found only in the central, $\sim 2°$ wide region of the map agrees much better with a single Gaussian[32]. This indicates that the additional signal is found at radii $\gtrsim 1°$, in agreement with the inferred ring.

The above arguments indicate that the local pixel significance should in fact be $\Delta s_j \sim -\mu_1 \simeq 1.2\sigma$ higher than it appears in the significance map (Figure 1a). This imposes a lower limit $\Delta S = 1.2(\mathsf{n}/\mathsf{n}_{0.2})^{1/2}\sigma$ to the correction factor needed in order to estimate the significance of an extended structure or of a cross-correlation signal (see §4) with respect to the true background. We conservatively use $\Delta S = 1.2\sigma$ for extended emission exceeding the beam size.

Another indication that such a correction is needed are the negative, $\lesssim -3\sigma$ significance regions, lying just outside the bright feature we identify as a ring. Assuming that the bright region is part of an extended, linear structure, this suggests that its local significance should be $\Delta s_j \gtrsim (3 + \mu_1)/2 \simeq 0.9\sigma$ higher than it appears.

Another way to assess the effect of wobble background subtraction is to apply it to a simulated cluster map. We thus normalize the γ-ray map of the simulated cluster derived in §6 below, add homogeneous poisson noise, introduce a $\mathsf{w} = 0.5°$ wobble-mode correction, and integrate over the $\theta = 0.2°$ beam. The normalization and background are chosen such that the final map thus obtained shows 4.0σ bright spots over a background comparable to the VERITAS background. For such parameters, a map identically prepared but with mean background, rather than wobble background subtraction, shows 6.1σ bright spots, implying a true significance $\sim 50\%$ higher than inferred in wobble-mode.

A γ-ray structure that extends over scales much greater than w would be largely erased by the wobble background subtraction. Hence, the above estimates provide only a lower limit to the correction needed to determine the significance of such a structure.

4. CROSS-CORRELATION SIGNALS AND WOBBLE-MODE CALIBRATION

Next, consider a cross-correlation between the VERITAS map s_j and some potential tracer of the virial shock, q_j. After binning the two maps onto some common grid,

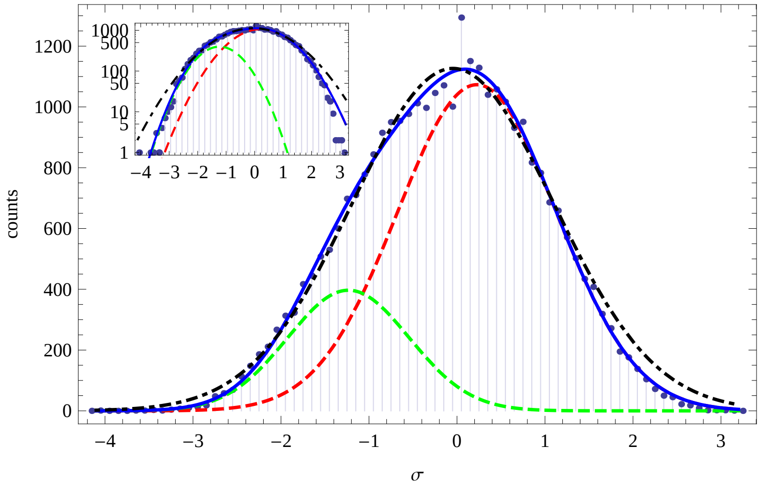

FIG. 4: **Histogram of pixel significance in the VERITAS map.** A single Gaussian function (dot-dashed) provides a marginal fit to the data. A much better fit is provided by the sum (solid) of two Gaussian functions (dashed); see text for function parameters. Inset: logarithmic histogram.

we compute the correlation as

$$C=\sum_{j=1}^{\mathsf{n}}\frac{(s_j-\mu_s)\,(q_j-\mu_q)}{\mathsf{n}^2\sigma_s\sigma_q\mathsf{n}_{0.2}^{1/2}}\ , \qquad (2)$$

where the means μ, standard deviations σ, and number of pixels n, pertain to the region being examined. The factor $\mathsf{n}_{0.2}$ accounts for the correlation between pixels within the $\theta = 0.2^\circ$ beam, ensuring that the result is approximately independent of the grid resolution. The significance of the correlation is determined by generating a large ($> \mathsf{n}^2$, converged) sample of maps with randomly swapped pixels, and computing the corresponding significance distribution.

Consider the effect wobble-mode background subtraction has on such cross-correlations. As in the significance estimation discussed in §3, any existing correlation is diminished because extended bright regions experience excessive background subtraction. However, the effect here is more severe, because background regions lying $\leq \mathsf{w}$ away from the bright structure are affected as well, appearing excessively faint. As such "dark edges" appear in the wobble-mode map but not in the tracers, the correlation is further diminished.

The effect of wobble-mode background subtraction on a cross-correlations signal can be crudely estimated by correlating mock tracers with simulated γ-ray maps, prepared with (*e.g.,* Figure 7) and without (*e.g.,* Figure 1b) wobble background subtraction. We generate mock tracers by adding random noise of various mean amplitude to the significance map of the simulated cluster, smoothed with a Gaussian filter of standard deviation r_q. The results are well-fit by a wobble correction factor

$$\Delta C \simeq 0.18e^{(r_q/0.2^\circ)}(d/5^\circ)C\ , \qquad (3)$$

where C is the nominal significance of the cross-correlation using the wobble-mode signal, $C+\Delta C$ is the true significance, and $\pi(d/2)^2$ is the solid angle involved.

For example, for the typical $r_q = 0.25^\circ$ of WMAP, the $C \simeq +2.8\sigma$ correlation found (see §7 below) between γ-ray and synchrotron emission outside the inner $b = 1^\circ$ ellipse bounding the γ-ray structure from below yields a corrected $C + \Delta C = +3.9\sigma$ confidence level. As pointed out in §3, these corrections are only lower limits if the γ-ray structure is more extended than the simulated ring used to derive Eq. (3).

5. NEGLIGIBLE GALACTIC CONTAMINATION

When averaged over large angular scales, the Galactic foreground anticipated above 220 GeV based on Fermi observations[31] is lower by at least a factor of a few than the ring signal (see §8). Moreover, Galactic signals on $\gtrsim \mathsf{w} = 0.5^\circ$ scales are efficiently removed from the VERITAS map by the wobble-mode background correction. Next, we show that no significant Galactic contamination on $\lesssim \mathsf{w}$ scales is expected in the VERITAS mosaic of Coma.

The main γ-ray Galactic foregrounds at intermediate latitudes arise from *(i)* inverse Compton emission from cosmic-ray (CR) electrons; *(ii)* relativistic bremsstrahlung of CR electrons with the interstellar plasma; and *(iii)* nucleon-nucleon scattering between CR ions and the interstellar medium. The CRs are unlikely to show significant structure on $< 0.5^\circ$ scales, as this would require < 10 pc magnetic fields at < 1 kpc distances. Moreover, synchrotron maps[33,34] show relatively very little emission from the Coma region. Therefore, the Galactic foreground on small scales is dominated by electron bremsstrahlung and by π^0 decay from nucleon collisions, both approximately following the distribution of gas along the line of sight.

Hence, we may estimate the Galactic contamination

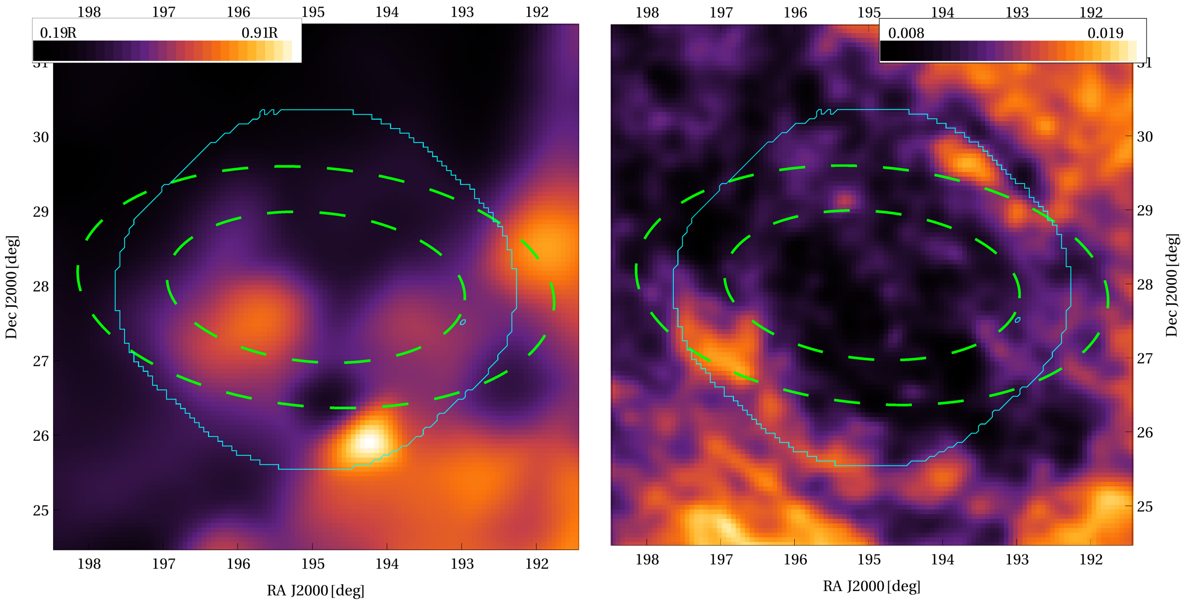

(a) Hα

(b) Dust

FIG. 5: **Tracers of Galactic foreground near Coma.**
The Hα full-sky map[35] (left; colorbar units: Rayleigh) and the SFD dust map[36] (right; colorbar: E(V-B) reddening) show only little Galactic structure in the region of the VERITAS mosaic (enclosed by cyan contour), and in particular towards the γ-ray ring (dashed green contours).

remaining in the VERITAS map using gas tracers, such as the full-Sky Hα[35] and infrared dust emission[36] maps (Figure 5). Both tracers indicate a very low level of Galactic structure in the Coma region, and towards the γ-ray ring in particular, with only minor structure found mainly in the East. We confirm this using a spectral linear regression of the seven-year WMAP data, outlined in §7. Both tracers show no positive correlation with the VERITAS map, ruling out any significant remaining Galactic contamination.

Note that synchrotron tracers should not be used here to estimate or eliminate the Galactic foreground. First, these tracers are inefficient as they follow the smooth CR electron distribution. More importantly, they include an interesting synchrotron signal from the Coma virial ring, as we argue in §7.

6. GAMMA-RAYS FROM A SIMULATED CLUSTER

The VERITAS signal can be assessed by comparing it to the γ-ray signature of a simulated Coma-like cluster in a ΛCDM simulation[3]. The γ-ray signal was computed by injecting relativistic electrons at the strong shocks of the simulation, with a Mach number-dependent power-law spectrum given by the Fermi diffusive shock acceleration model. These electrons were assumed to carry a fraction ξ_e of the thermal post-shock energy; see §8 for details. We choose the richest cluster in the $(200\text{ Mpc})^3$ simulation box, found[7] to have a Coma-like mass $\sim 10^{15}M_\odot$ and temperature $T\sim 8$ keV.

The simulated virial shock (Figure 1b) has an elliptic structure, elongated towards the main LSS filament (Figure 6a), with semi-minor axis $b\simeq 1.3°$ and semi-major axis $a\simeq 2.5°$ (at the distance of Coma); the average <220 GeV spectral index is $p\simeq 2.05$. The shock elongation, the morphology of the surrounding filaments, and the enhanced accretion towards the main filament, suggest a prolate geometry aligned with the main filament feeding the cluster. Unrelaxed, merger clusters such as Coma are indeed known to preferentially be prolate[37].

The center of the simulated cluster is determined by the peak density. The simulated map is rotated about this point such that the main simulated LSS filament coincides with the $\phi\sim -5°$ orientation of the SDSS filament and the ROSAT ellipse. By coincidence, the agreement between the simulated filaments and the SDSS map remains fairly good even far from the cluster, if the simulated map is inverted along the semi-major axis of the virial shock (Figure 6).

The simulated γ-ray signal shows a positive correlation with the VERITAS map (Figure 1), at the 3.7σ confidence level (4.9σ after correcting for the excessive wobble-mode background subtraction; see §3). The correlation remains strong, $>3.5\sigma$ ($>4.7\sigma$), if the maps are rotated by $<5°$ with respect to each other. The extent of the virial shock may be somewhat overestimated by the adiabatic, smooth particle hydrodynamics (SPH) simulation. Indeed, the correlation strengthens to 4.1σ

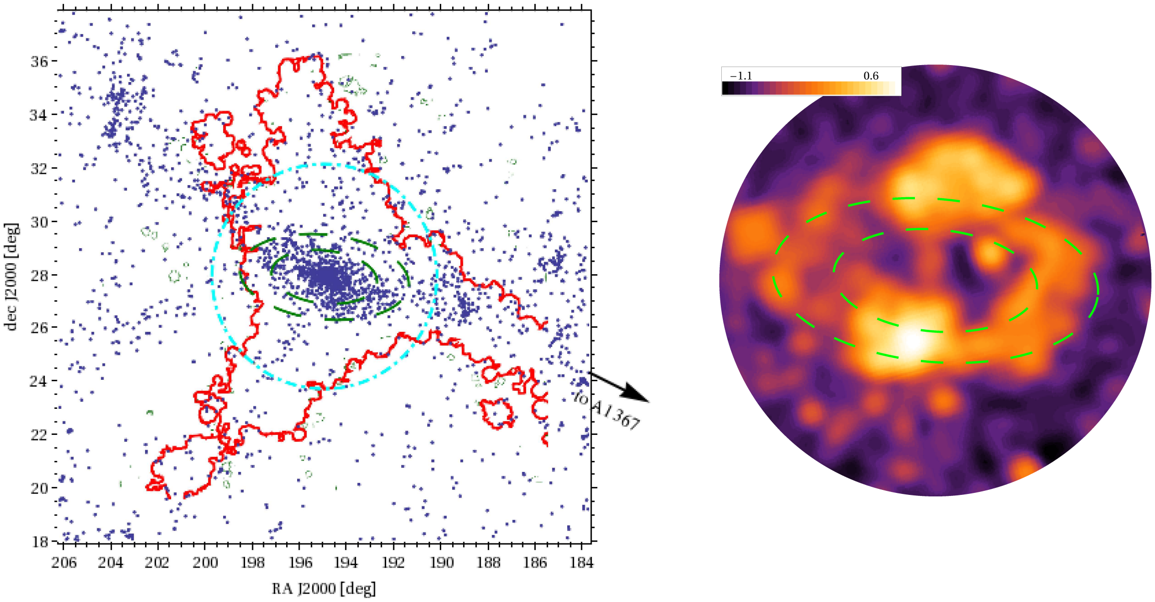

(a) SDSS galaxies with simulated LSS filaments (b) Corresponding simulated γ-ray map

FIG. 6: **The LSS environment of Coma.**
Left: SDSS galaxies at redshift $0.018 < z < 0.028$ near Coma. The simulation roughly reproduces the filamentary structure near Coma, especially when reflected about the semi-major axis of the virial shock (solid red contours show the density-weighted $T = 1$ keV gas in a 4.4 Mpc thick slice through the simulation box[3]). *Right:* γ-ray map for $\xi_e\dot{m} = 5\%$, showing the > 220 GeV brightness as $\log_{10}(J/10^{-8}\ \mathrm{cm}^{-2}\ \mathrm{s}^{-1}\ \mathrm{ster}^{-1})$ after said reflection. Elliptic dashed contours from Figure 1a are superimposed, and the region shown in the right panel is marked by a dot-dashed circle.

(5.3σ) if the simulated map is resized by a factor 0.9.

The mass accretion rate $\dot{M}$ of the cluster, normalized by the mass-to-Hubble time ratio in the dimensionless parameter $\dot{m} \equiv \dot{M}/(MH)$, varies among clusters and fluctuates in time, and is found[7] to be somewhat low when averaged over the simulated cluster, $\dot{m} \simeq 0.3$. The γ-ray map shown in Figure 1b corresponds to normalized average accretion rate $\dot{m} = 1$, and an acceleration efficiency $\xi_e = 5\%$. Equivalently, we may examine the accretion rate of the total thermal energy U_{th}, using the dimensionless parameter $\dot{u} \equiv \dot{U}_{th}/(U_{th}H)$. In the simulation, we find[3,7] $\dot{u} \simeq \dot{m}$, although slightly larger, $\dot{u} = (5/3)\dot{m}$ values arise in a simple isothermal sphere model[4].

7. SIGNIFICANT CROSS-CORRELATIONS BETWEEN γ-RAY AND RADIO SIGNALS

In order to quantify the coincidence between γ-ray and radio signals, we analyze the WMAP seven-year, full-sky maps[21]. We use a simple spectral decomposition of the five WMAP bands into synchrotron and SZ maps, avoiding any spatial masking which may complicate the comparison to the VERITAS map.

The synchrotron spectrum is approximated as a pure power-law, with brightness $I_\nu \propto \nu^\alpha$ and spectral index $\alpha = -1.2$, typical of cluster radio sources; the results are not sensitive to the precise spectrum for $-2 \lesssim \alpha \lesssim -1$. The SZ signal is clear in the central parts of Coma, but is difficult to spectrally separate from the CMB fluctuations at large radii[21]. For simplicity, we leave these CMB fluctuations in the SZ map, thus somewhat diluting any correlations with the VERITAS map.

In general, the WMAP data includes non-negligible foregrounds from Galactic synchrotron, dust and free-free emission[38], which are strong towards the Galactic plane and in principal should be removed. However, as discussed in §5, these signals are particularly weak in the Coma region (Figure 5), are spatially too smooth (in particular the synchrotron foreground) to have a γ-ray counterpart surviving the wobble-mode background removal, and their tracers do not correlate with the VERITAS map.

Moreover, the extragalactic synchrotron signal cannot be separated from the Galactic $\alpha \simeq -1$ synchrotron, $\alpha \simeq -0.7$ dust, and $\alpha \simeq -0.35$ free-free signals, using spectral regression alone, in particular considering the varying synchrotron spectral index in the cluster radio sources. Therefore, we leave these faint and probably smooth Galactic contaminations in our synchrotron extragalactic tracer. This only dilutes the correlations between this tracer and the VERITAS map, as the Galactic signals show no positive correlations with the latter.

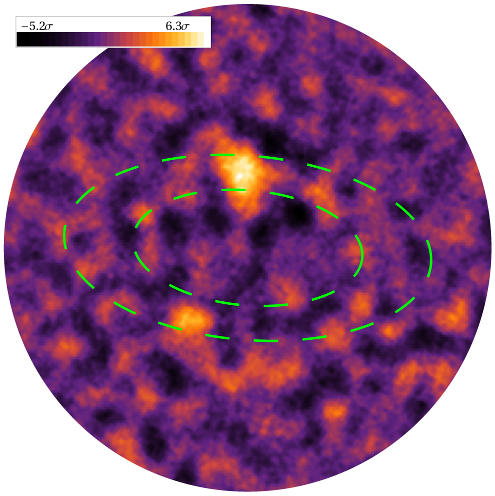

FIG. 7: **Wobble-mode background-subtracted γ-ray map of the simulated cluster.** The map corresponds to the VERITAS parameters: $\Delta t = 18.6$ hour integration, $A = 4\times 10^8\,\mathrm{cm}^2$ effective area, and 90% Poisson noise. While the bright spots are $\sim 3\sigma$ for $\xi_e\dot{m} = 5\%$, here we use $\xi_e\dot{m} = 50\%$ to also show the dimmer Western edge.

Therefore, we fit the five WMAP channels by

$$\begin{aligned}\Delta T &= T - T_{\mathrm{cmb}} \qquad (4)\\ &= y\left[\tilde{\nu}\coth\left(\frac{\tilde{\nu}}{2}\right) - 4\right] + T_{\mathrm{syn}}\left(\frac{\nu}{\nu_0}\right)^{-3.2},\end{aligned}$$

where $\tilde{\nu} = h\nu/k_B T_{\mathrm{cmb}}$ is the dimensionless frequency and y is the Comptonization parameter. The low-frequency SZ temperature shift $\Delta T_{\mathrm{sz}} = -2y$ and the synchrotron brightness temperature T_{syn} (at the arbitrary frequency ν_0) are used as fit parameters, giving the tracer maps (Figure 8).

Next, we compute the cross-correlation amplitudes of the VERITAS data with these ΔT_{sz} and T_{syn} maps. On average, the VERITAS data show no correlation with the synchrotron map, and an insignificant, -1.0σ (-1.6σ) anti-correlation with the SZ map (*i.e.* a positive correlation with the y-parameter). Here and below, results in parenthesis are the conservative confidence levels after correcting for the wobble-mode background subtraction, as described in §4.

Features seen in both SZ and synchrotron maps are more pronounced in the Western part of the cluster, possibly due to some Eastern foreground (*e.g.*, see Figure 5a) or CMB fluctuation. Consequently, for RA < 195.3 (no more than 0.5° East of the cluster's center), the SZ anti-correlation strengthens to -1.6σ (-2.3σ). Note that this signal does not arise from the spatial separation between the central SZ decrement and the peripheral γ-ray ring, as this would correspond to a positive correlation here.

More importantly, when we split the data into two regions, outside and inside the inner $b = 1°$ ellipse bounding the γ-ray signal, correlations emerge between γ-rays and both radio signals. Outside this inner ellipse, i.e. along the γ-ray ring, the VERITAS map correlates with the synchrotron map at the $+2.8\sigma$ ($+3.9\sigma$) confidence level, and anti-correlates with the SZ map at the -2.6σ (-3.6σ) level. The signal is dominated by the Western half of the ring, where these correlations strengthen to $+3.2\sigma$ ($+4.1\sigma$) with the synchrotron and -3.9σ (-5.0σ) with the SZ. The results depend somewhat on the precise region examined. For example, including the 0.5° region east of the center, the synchrotron correlation strengthens to $+3.5\sigma$ ($+4.6\sigma$) while the SZ correlation remains unchanged.

Within the $b = 1°$ ellipse, the VERITAS map does not correlate with the SZ signal, but does show a -1.9σ (-2.7σ) anti-correlation with the synchrotron map, mainly in the Western part, where it reaches -2.2σ (-2.8σ). The inner anti-correlation between the VERITAS and synchrotron maps, evident in the γ-ray underluminous radio halo and radio relic, and their outer positive correlation, are illustrated in Figure 9.

In the periphery of the cluster, the positive correlation between the VERITAS map and the synchrotron signal agrees with predictions for the coincident inverse-Compton and synchrotron emission from the same relativistic, shock-accelerated electrons, as we show in §8 and §9 below. The anti-correlation with the SZ map agrees with the anticipated SZ signal from the thermal gas, expected to cutoff sharply as the thermal pressure drops beyond the virial shock, as shown in §9.

In the inner parts of the cluster, an anti-correlation between γ-ray and synchrotron radiation was anticipated in secondary electron models, where electrons are continuously injected into the ICM in both strongly and weakly magnetized regions[22]. Here, electrons magnetized above (below) $B_{\mathrm{cmb}} \equiv (8\pi u_{\mathrm{cmb}})^{1/2} \sim 3\,\mu\mathrm{G}$, where u_{cmb} is the CMB energy density, lose most of their energy to synchrotron (inverse-Compton) radiation in the radio (γ-ray) band[26], leading to alternating radio- and γ-ray-bright regions, as discussed in §10.

8. THE OBSERVED γ-RAY SIGNAL AGREES WITH PREDICTIONS FOR AN $\xi_e\dot{m} \sim 5\%$ ELECTRON INJECTION RATE

Cluster virial shocks last for long, $\sim H^{-1}$ Hubble timescales, and are strong, in particular where cold gas accretes from the voids and the Mach number squared is $\gg 10$. Therefore, such shocks are thought to accelerate a flat, $dn/d\epsilon \propto \epsilon^{-2}$ spectrum (constant energy per logarithmic energy interval) of relativistic electrons up to high, cooling-limited energies. The dominant cooling process here is Compton scattering off CMB photons, implying

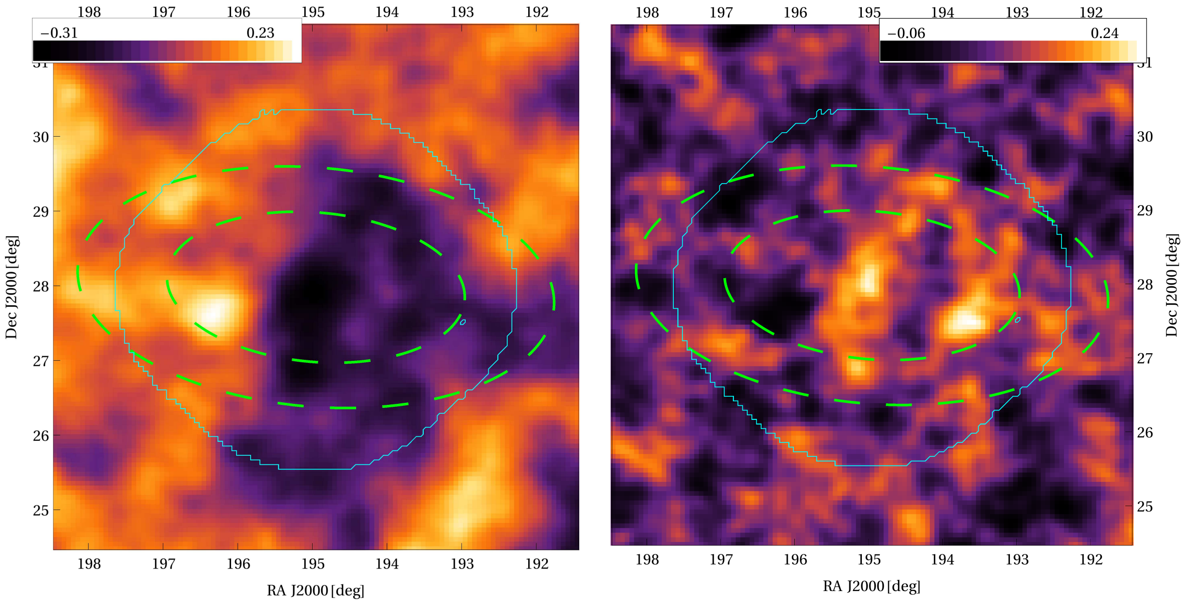

(a) Thermal SZ

(b) Synchrotron

FIG. 8: **Radio maps of the Coma region.**
Thermal SZ (left; colorbar is the low-frequency $\Delta T_{\rm sz} = -2y$ in mK) and synchrotron (right; colorbar is $T_{\rm syn}(\nu/23\text{ GHz})^{3.2}$ in mK) maps, spectrally extracted from the WMAP seven-year all sky map[21]. The dashed curves, showing the γ-ray bright region, are the same as in Figure 1a, and the cyan contours show the VERITAS mosaic region.

an electron energy cutoff[1]

$$\epsilon_{max} \simeq \frac{\Gamma+1}{2} m_e c \sqrt{\frac{3eBk_BT}{(\Gamma-1)m_p\sigma_T u_{\rm cmb}}} \simeq 60(T_{10}B_{0.1})^{1/2}\text{ TeV} , \tag{5}$$

where $k_BT = 10T_{10}$ keV and $B = 0.1B_{0.1}$ μG are the temperature and magnetic field amplitude downstream of the shock. Here, e and m_e are the electron charge and mass, σ_T is the Thompson cross section, and c is the sound velocity. The photon energy $E \sim 220$ GeV which maximizes the VERITAS sensitivity corresponds[13] to electrons with energy $\epsilon \simeq (E/3k_BT_{\rm cmb})^{1/2}m_ec^2 \simeq 9$ TeV, below but not far from the estimated cutoff.

The main uncertainty in modelling the nonthermal emission from a virial shock stems from the presently poor understanding of particle acceleration and magnetization in collisionless shocks. The inverse-Compton emission from the shock can be estimated by assuming that a fraction $\xi_e = 0.05\xi_{e,5}$ of the post-shock thermal energy is deposited in relativistic electrons. Electrons with energies $\gg 100$ MeV cool quickly, in a narrow shell behind the shock, so the logarithmic emissivity per unit surface area of the shock is

$$E^2\frac{d^3N}{dt\,dA\,dE} \simeq \frac{3\xi_e vnk_BT}{4\ln(\epsilon_{max}/m_ec^2)} \simeq 10^{-8}\xi_{e,5}n_{-5}T_{10}^{3/2}\text{ erg s}^{-1}\text{ cm}^{-2} , \tag{6}$$

where $n = 10^{-5}n_{-5}$ cm^{-3} is the (thermal) electron number density, and $v = (k_BT/12\mu)^{1/2}$ is the downstream velocity.

The γ-ray signal from a Coma-like cluster can be computed using Eq. (6) in the framework of a cosmological simulation[3,5], without introducing additional free parameters. However, the comparison between simulated and observed clusters is complicated by a secondary uncertainty, involving the local accretion rate of the cluster. This rate varies spatially along the shock front, fluctuates in time, and differs even among similar clusters as a function of their specific environment. We parameterize the average accretion rate using the dimensionless variable

$$\dot{m} \equiv \frac{\dot{M}}{MH} \simeq \frac{4\pi R^2\mu nv}{f_bMH} , \tag{7}$$

where here we assumed a spherical shock of radius R. In the β-model discussed in Appendix A, $\dot{m} = 1.4$, and in the simulated cluster[7] $\dot{m} \simeq 0.3$. These are averaged quantities, with strong local fluctuations seen in simulations and expected in practice.

Consider a planar cut parallel to the line of sight, along which the virial shock is approximately a ring of radius R and of negligible thickness. A beam that intersects the cut at distances $\{r_1, r_2\} < R$ from the center covers a shock segment of length $2R|\arcsin(r_2/R) - \arcsin(r_1/R)|$. Therefore, at the near edge of a long cylindrical shock of angular radius ψ, a beam of area θ^2 would detect $> E$

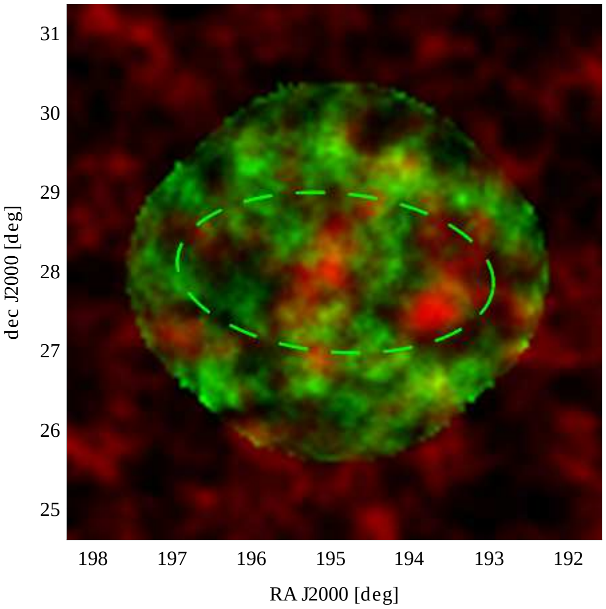

FIG. 9:
Composite γ-ray and synchrotron emission. Superimposed VERITAS map (green; colorbar range: -3.4σ to $+3.0\sigma$) and synchrotron map (red; spectrally extracted from the WMAP 7-year full sky-map; colorbar range: -1.3 to $+5.4(\nu/\mathrm{GHz})^{3.2}$ K), showing a positive correlation (yellow) outside the inner edge of the γ-ray ring (dashed contour) and an anti-correlation (spatially separated green and red, the latter dominated by the radio halo and relic) inside the ring.

energy photons with number flux

$$J(>E) \simeq \frac{\pi - 2\arcsin\left(1-\theta/\psi\right)}{4\pi(1+z)^4\theta/\psi} E\frac{d^3N}{dt\,dA\,dE} \; . \tag{8}$$

A similar result is expected in the prolate shock inferred in Coma, where for the VERITAS map

$$J(>220\text{ GeV}) \simeq 2\times10^{-8}\left(\frac{\psi}{10\theta}\right)^{1/2}\xi_{e,5}n_{-5} \times T_{10}^{3/2}\text{ s}^{-1}\text{ cm}^{-2}\text{ ster}^{-1} \; . \tag{9}$$

In the isothermal β-model, this may be written as $J(>220\text{ GeV}) \simeq 5\times10^{-8}\xi_{e,5}\dot{m}\text{ s}^{-1}\text{ cm}^{-2}\text{ ster}^{-1}$.

In order to compare this estimate with the γ-ray structure seen in the VERITAS map, recall that a 1σ fluctuation corresponds to an excess of $N_\sigma = N_{0.2}^{1/2} \simeq 32$ photons with $E \gtrsim 220$ GeV in a beam of radius $\theta = 0.2°$. The map was produced by a $t = 18.6$ hour exposure[13], with an $A \simeq 4\times10^8\text{ cm}^2$ effective area (at ~ 220 GeV, see[39]). A 1σ signal in the beam therefore corresponds to a photon flux

$$J_{1\sigma} \simeq \frac{N_\sigma}{\pi\theta^2 tA} \simeq 3.1\times10^{-8}\text{ s}^{-1}\text{ cm}^{-2}\text{ ster}^{-1} \; . \tag{10}$$

The average signal inferred from the histogram (Figure 4), $\mu_2 - \mu_1 \simeq 1.4\sigma$, is thus comparable to the predicted signal in Eq. (9) for standard parameters.

The agreement between the predicted (Eq. 9) and observed (Eq. 10) γ-ray flux, and the similar significance of the γ-ray features in the observed (Figure 1a) and simulated (Figure 1b) maps, suggest that to within an uncertainty factor of a few, $\xi_e\dot{m} \simeq 5\%$. Localized regions with $\sim 3\sigma$ detection, and possibly brighter emission masked by the wobble-mode background subtraction, suggest that at least locally the product $\xi_e\dot{m}$ can exceed its inferred average value by a factor of a few.

The total flux from the virial shock can be estimated by taking $\theta \to 2\psi$ in Eq. (8), and integrating over the solid angle enclosed by the shock. For a cylindrical ring of radius b and length $\tilde{\zeta}b$, this gives

$$\begin{aligned} F(>E) &\simeq \frac{2b^2\tilde{\zeta}}{4(1+z)^4}E\frac{d^3N}{dt\,dA\,dE} \\ &\simeq 10^{-9}\frac{\tilde{\zeta}b_1^2\xi_{e,5}n_{-5}T_{10}^{3/2}}{E_1(1+z)^4}\text{ s}^{-1}\text{ cm}^{-2} \; , \end{aligned} \tag{11}$$

where $b_1 \equiv b/1°$ and $E_1 \equiv E/1$ GeV. For the VERITAS band and $b = 1.3°$, we use the isothermal β-model to obtain $F(>220\text{ GeV}) \simeq 3\times10^{-11}\tilde{\zeta}\xi_{e,5}\dot{m}\text{ s}^{-1}\text{ cm}^{-2}$. Calibrating the free parameters against the local 1σ VERITAS flux (Eq. 10), this becomes $F(>220\text{ GeV}) \simeq 2\times10^{-11}\tilde{\zeta}\text{ s}^{-1}\text{ cm}^{-2}$.

Extrapolating the VERITAS-calibrated signal to the EGRET band (assuming a flat spectrum), yields $F(>100\text{ MeV}) \simeq 4\times10^{-8}\tilde{\zeta}\text{ s}^{-1}\text{ cm}^{-2}$, comparable to the $4\times10^{-8}\text{ s}^{-1}\text{ cm}^{-2}$ EGRET upper limit on emission from Coma[10,11]. The corresponding $F(>200\text{ MeV}) \simeq 2\times10^{-8}\tilde{\zeta}\text{ s}^{-1}\text{ cm}^{-2}$ exceeds the $5\times10^{-9}\text{ s}^{-1}\text{ cm}^{-2}$ upper limit imposed by Fermi[12], but this limit was obtained using an aperture optimized for emission from the central, X-ray bright region of the cluster. Note that at such low energies, the Galactic foreground is not negligible, and both instruments lack the high angular resolution of VERITAS essential in order to identify the ring and avoid foreground contamination.

The above analysis assumed a flat spectrum of accelerated electrons, leading to a flat ($p = 2$) photon spectrum. Indeed, comparing the VERITAS measurement with the EGRET upper limit implies that the photon spectral index between 100 MeV and 220 GeV cannot be much softer than $p = 2.1$. As the VERITAS measurement probes only photons near 220 GeV, the above estimates strictly pertain to electrons in energies near 10 TeV. Here, we find a logarithmic electron injection efficiency

$$\dot{m}\epsilon\frac{d\xi_e}{d\epsilon} \simeq \frac{\xi_e\dot{m}}{\ln(\epsilon_{max}/\epsilon_{min})} \simeq 0.3\% \; . \tag{12}$$

9. THE SYNCHROTRON AND SZ SIGNALS AGREE WITH PREDICTIONS FOR $\xi_B \sim 1\%$ MAGNETIZATION

The same electrons that scatter CMB photons up to the γ-ray band also emit synchrotron radiation, as they gyrate in the shock amplified magnetic fields. The ratio between radio and γ-ray emission from a strong virial shock is approximately given by the ratio between magnetic and CMB energy densities,

$$\frac{\nu I_\nu}{EJ(>E)} \simeq \frac{B^2/8\pi}{u_{\rm cmb}} \, . \tag{13}$$

In order to compute the synchrotron signal, some assumption must be made concerning the magnetic field behind the shock. Typically[4,7], one assumes that a fraction $\xi_B \equiv 0.01\xi_{B,1}$ of the thermal energy is deposited in downstream magnetic fields, based on observations of supernova remnant shocks; some magnetization is also needed to accelerate the γ-ray emitting electrons. However, this assumption was not tested so far near the virial shock, and the value of ξ_B is not well constrained.

We may use the coincident γ-ray and radio measurements to estimate the magnetic field at the shock. The strongest signal is found in the lowest WMAP frequency, $\nu = 23$ GHz, where bright spots along the shock show $T_{\rm syn} \simeq 0.1$ mK, corresponding to a brightness

$$\nu I_\nu = 2\frac{\nu^3}{c^2} k_B T_{\rm syn} \simeq 10^{-9} \mbox{ erg s}^{-1} \mbox{ cm}^{-2} \mbox{ ster}^{-1} \, . \tag{14}$$

The same bright spots are detected by VERITAS at $\sim 3\sigma$, corresponding to $EJ(>E) \simeq 3.2 \times 10^{-8}$ erg s^{-1} cm^{-2} ster^{-1}. Equation (13) then yields $B \simeq 0.4\ \mu$G, which according to the β-model corresponds to $\xi_B \simeq 0.5\%$.

We may use the SZ signal near the shock to test the above estimates. For example, at $\nu = 23$ GHz one expects the ratio between the synchrotron emission and the SZ decrement to be $T_{\rm syn}/\Delta T_{\rm sz} \simeq -0.3\xi_{e,5}\xi_{B,1}\dot{m}$ for an isothermal sphere distribution[4,7], and $T_{\rm syn}/\Delta T_{\rm sz} \simeq -0.5\xi_{e,5}\xi_{B,1}$ for a β-model (see Appendix A).

Inspecting the coincident synchrotron ($T_{\rm syn} \sim 0.1$ mK at 23 GHz) and SZ ($\Delta T_{\rm sz} \sim -0.2$ mK) signals measured along the γ-ray ring, we find that $\Delta T_{\rm syn}/\Delta T_{\rm sz} \simeq -0.5$. This supports the above estimates $\xi_e \dot{m} \simeq 5\%$, and $\xi_B \simeq 1\%$. Note that the parameter ξ_B refers to the magnetic energy weighted over the relativistic electron distribution, and so is elevated by clumping effects[7].

10. IN THE INNER REGIONS, THE γ-RAY–SYNCHROTRON ANTI-CORRELATION SUPPORTS STRONG MAGNETIZATION AND HADRONIC INJECTION

Within $b = 1°$, we find an anti-correlation between γ-rays and synchrotron emission. This signal is not highly significant (-2.2σ and -2.8σ, before and after correcting for wobble background removal), so deeper observations are needed to clarify its nature. Here we consider the implications of the anti-correlation assuming it is indeed real. In such a case, as the synchrotron signal involved is dominated by the radio halo and radio relic, some of the VERITAS signal must arise from the inner ICM, well inside the virial radius.

In the radio band, Coma is a classical example of a merging cluster, harboring both an extended radio halo and a peripheral radio relic[16]. The $\gtrsim$ Mpc size of such radio halos implies an ongoing injection of relativistic electrons, but it is debated whether they arise from hadronic collisions involving CR ions (secondary models[22,25,26,40]) or from in-situ (re)acceleration in weak shocks or turbulence (primary models[23,24,41]). Secondary models can also explain radio relics[22] and minihalos[27] as arising from the same distribution of CR protons, if the latter are homogeneously distributed[22]. Here, radio-bright regions correspond to strong, $B \gtrsim B_{\rm cmb}$ magnetic fields. The existence of such strongly magnetized regions is also being debated, in Coma[42,43] and in other clusters[22,44–46].

In secondary models, electron injection is an ongoing process, proportional to the gas density but largely independent of shocks, turbulence, and other changes in the flow. Therefore, the sum of synchrotron and inverse-Compton emission from the ICM varies slowly across the cluster, whereas their ratio can show strong variations, proportional to $(B/B_{\rm cmb})^2$, leading to a radio–γ-ray anti-correlation. In contrast, in primary models, the electrons are injected only locally, in shocks or turbulence where the magnetic field is amplified, and cool long before the magnetic field can decay. Hence, a positive correlation is expected here between synchrotron and γ-ray signals; inverse-Compton emission far from the radio sources is expected to be negligible.

In both secondary and primary models, γ-ray emission is expected also from π^0 decay, following CR ion collisions with the ambient nucleons. This signal is expected to be smoother than the inverse-Compton emission, and so more susceptible to wobble-mode background subtraction, in particular if the CRs are distributed homogeneously, as inferred from hadronic radio models[22]. For example, in a β-model with homogeneous CR ions, wobble-mode removes $> 50\%$ of the signal in the central $0.2°$ beam, which corresponds to the magnetized core, and $> 90\%$ of the signal beyond $\psi = 0.3°$. The π^0 signal, independent of the local magnetic field and stronger in the center, should positively correlate with the synchrotron map, which is dominated by the central radio halo. It cannot account for the anti-correlation presently observed.

Therefore, the inner γ-ray–synchrotron anti-correlation, if confirmed, supports the notion of magnetized, $\gtrsim 3\ \mu$G regions in the ICM, and favors a secondary electron injection model. Here, the presence of a weak γ-ray signal far from the center (but inward of the virial shock) supports a homogeneous CR proton distribution. In non-magnetized regions, the $T_{\rm syn}(23\mbox{ GHz}) \sim 0.2$ mK synchrotron signals from the radio halo and relic translate to an inverse-Compton flux $J(> 220\mbox{ GeV}) \simeq 3\times 10^{-9}$ s^{-1} cm^{-2} ster^{-1}. By Eq. (10), this corresponds to an $s_j \simeq 0.1\sigma$ VERITAS significance per $\theta = 0.2°$ beam, so γ-ray emission around the core can plausibly lead to the observed anti-correlation.

Integrated within a $b = 1^\circ, \zeta = 3$ ellipse, emission from secondary electrons corresponds to an $S \simeq 0.4\sigma$ nominal VERITAS signal, assuming homogeneous CR ions and a β-model gas distribution. Such a signal can be further tested in a deeper γ-ray observation. If wobble-mode corrections can be minimized, the (~ 4 times stronger[47]) π^0 signal may be measured as well.

11. SUMMARY AND DISCUSSION

We analyze the VERITAS mosaic (Figure 1a) of the Coma cluster, and find a large-scale, extended γ-ray feature around the cluster. It is best described as an elongated ($\zeta \gtrsim 3$), thick ($\Delta b \gtrsim 0.5^\circ$) elliptical ring, with semi-minor axis $b \simeq 1.3^\circ$ (Figure 2), oriented approximately along the East-West direction ($\phi \sim -5^\circ$; Figure 3), towards the LSS filament connecting Coma with Abell 1367 (Figure 6a). The γ-ray ring is seen at a nominal 3.3σ confidence level, but comparison with mock VERITAS noise maps implies a higher, 4.5σ confidence. Further correcting for excessive wobble-mode background subtraction, we conclude that the ring presents with a confidence level of at least 5.7σ. If we do not assume a-priori that the ring is aligned with the LSS filament, the significance becomes 4.2σ ($\geq 5.4\sigma$ corrected). Our wobble-mode corrections, derived in §3 and §4 (see Figure 4, and Eq. 3), are quite conservative.

The size and morphology of the γ-ray ring agree with predictions for the signature of the virial shock, produced as shock-accelerated electrons inverse Compton-scatter CMB photons. The VERITAS map thus correlates with a normalized simulated γ-ray map of a Coma-like cluster (Figure 1b), once the main LSS filaments are similarly oriented (Figure 6), at a 3.7σ (4.9σ) confidence (no free parameters; see Figure 7). The best fit is obtained for ellipticity $\zeta \simeq 4.5$, but we cannot rule out a cylindrical shock parallel to the LSS filament. The brightness of the signal agrees with predictions as well, provided that the rate of relativistic electron energy deposition is $\xi_e \dot{m} \simeq 5\%$ of the thermal energy per Hubble time (within a factor of a few).

Interestingly, a 3σ signal found[9] by stacking the EGRET data around 447 rich clusters corresponds, when compared with source number counts computed analytically[4] and using cosmological simulations[3], to an average $\xi_{e,5}\dot{m} \simeq 4\%$, in agreement with the value we infer in Coma.

Inverse-Compton emission from virial shocks can explain the hard X-ray signals observed in several clusters[6], provided that $\xi_e \lesssim 10\%$. For example, $\xi_e \dot{m} \simeq 4\%$ was recently inferred from hard X-ray emission from a LSS filament[20]. The VERITAS ring corresponds to a $\sim 5\tilde{\zeta}$ eV s^{-1} cm^{-2} flux at 20–80 keV energies (assuming a flat spectrum), accounting for the (8.1 ± 2.5) eV s^{-1} cm^{-2} hard X-ray signal observed[19]. High resolution observations in hard X-rays, in particular with NuSTAR, should resolve the virial ring in Coma, and detect virial shocks in many other clusters.

An analysis of the WMAP seven-year data reveals a positive correlation between the γ-ray ring and synchrotron emission (Figures 8b and 9), at the 2.8σ (3.9σ) confidence level, and an anti-correlation with the SZ map (Figure 8a) at -2.6σ (-3.6σ). The radio signals are clearer in the Western half of the ring, towards the LSS filament, where the correlations reach 3.5σ (4.6σ) and -3.9σ (-5.0σ), respectively. They agree with predictions for the synchrotron emission from the γ-ray emitting electrons and for the SZ decline with thermal pressure beyond the shock, if the downstream magnetic field is $B \simeq 0.4\ \mu$G, corresponding to $\xi_B \simeq 0.5\%$ magnetization (within a factor of a few).

The SZ signal we find, extending in some parts out to $\psi \simeq 2.3^\circ$ away from the center, agrees with the SZ detections by WMAP[21] and Planck[17]. However, the peripheral synchrotron signal coincident with the γ-rays and with the SZ cutoff was not reported so far. The γ-ray ring and these radio features are much farther out than the $\psi \simeq 0.5^\circ$ weak shocks seen in X-ray, radio[16], and SZ[17] data.

Inward of the ring, the VERITAS map shows a -1.9σ (-2.7σ) anti-correlation with the synchrotron map, stronger in the Western region where $C = -2.2\sigma$ (-2.8σ). This is evident in the radio halo and radio relic, which appear underluminous in γ-rays (Figure 9). Such a signal was predicted in models where relativistic electrons are injected into the ICM continuously, in both strongly and weakly magnetized regions which consequently appear radio bright/γ-ray faint and vice versa. While the present signal is weak and requires confirmation, it is consistent with analytic estimates. The extent of the anti-correlation and its magnitude support secondary electron injection by collisions of cosmic-ray protons with the ambient nucleons, and favor a homogeneous CR distribution.

A VERITAS observation deeper than the present 18.6 hour exposure would decisively test our results, in particular if wobble-mode corrections can be avoided or minimized, for example by using a larger, $\mathsf{w} > 1^\circ$ wobble radius. This would allow for a more precise reconstruction of the virial shock structure and a determination of variations in the electron deposition rate along the shock front. Such data would be valuable in the study of large-scale structure formation at low redshift, mapping the feeding pattern of Coma, probing the surrounding voids, the Coma–Abell 1367 filament, and other LSS filaments, and tracing the warm-hot intergalactic medium (WHIM) immediately behind the shock.

Such a deep observation would test the anti-correlation we find between γ-ray and radio maps at small, $b \lesssim 1^\circ$ radii. A significant anti-correlation would confirm the hadronic, secondary electron model for cluster radio sources, and provide a direct measure of magnetic variations in the ICM. A deep observation would thus probe the CR proton distribution out to large radii, address the origin of these protons, and in particular place an upper limit on proton acceleration in the virial shock.

Observations at lower energies, for example using the $\sim$ 50 GeV MAGIC Čerenkov telescopes[48], should be able to utilize the higher photon flux to clearly identify the γ-ray ring. At yet lower energies, the Fermi γ-ray space telescope is marginally sensitive to the signal at $\lesssim 1$ GeV, but it may be challenging to resolve the shock structure with the $\gtrsim 1^\circ$ (68% containment) point spread function[49].

The VERITAS energy threshold, $E \simeq 220$ GeV, is not far below the expected photon cutoff, $E_{max} \simeq 10 T_{10} B_{0.1}$ TeV. Observations at higher energies would become increasingly sensitive to this cutoff, thus probing the conditions at the shock and the nature of particle acceleration, although pair production off the infrared background also becomes important at such energies[50]. Interestingly, no evidence for extended emission was found in a 1.1 TeV observation of Coma by the HESS telescopes[28]. Despite the higher energy threshold and the shorter, 8.2 hour observation, it was only ~ 2.3 times less sensitive than the VERITAS observation (assuming a flat spectrum), thanks to the larger effective area[51], $\sim 2\times 10^9$ cm^2. The HESS map shows no significant signal or correlation with the VERITAS data, but the γ-ray ring may well be shallowly buried under the noise. Note that the optical depth of the HESS photons due to pair production off the infrared background, estimated[50] as $\tau \simeq 0.2$, may not be negligible.

Finally, consider the contribution of cluster virial shocks to the extragalactic γ-ray and radio backgrounds. These components were computed analytically[1–3], and calibrated numerically using cosmological simulations[3,5,7]. While the main model parameters $\xi_e \dot{m}$ and ξ_B are likely to fluctuate within clusters and vary among different clusters, it is instructive to adopt the values inferred in Coma as typical. An accretion rate $\dot{m} \simeq 1$ is intermediate between the analytic model[4] and the low redshift result of numerical simulations[3]. Normalizing all clusters by this value, we obtain a diffuse γ-ray component $E^2 dJ/dE \simeq 0.3(\xi_e \dot{m}/5\%)$ keV s^{-1} cm^{-2} ster^{-1}, dominating the extragalactic background[29]. In the radio, the revised parametrization yields a $\nu I_\nu \sim 3\times 10^{-11}(\xi_e\dot{m}/5\%)(\xi_B/1\%)$ erg s^{-1} cm^{-2} ster^{-1} synchrotron signal, dominating the extragalactic low frequency radio background[7]. It is observable through $\delta T_l \simeq 1(\nu/\mathrm{GHz})^{-3}$ K fluctuations at multipoles $400 \lesssim l \lesssim 2000$ with present interferometers such as LOFAR and EVLA.

ACKNOWLEDGMENTS

We thank Ido Reiss and Boaz Katz for useful discussions. The research of UK has received funding from the European Union Seventh Framework Programme (FP7/2007-2013) under grant agreement n$^{\mathrm{o}}$ PCIG09-GA-2011-293975.

Appendix A: β model for the shock

An analytic model for emission from the virial shock requires some assumptions specifying the gas distribution. Simple choices include an isothermal sphere[4] or a isothermal β-model[47], the latter of which we discuss below.

In our simple model, it is assumed that *(i)* the electron number density is approximately given by

$$n(\mathbf{r}) = n_0 \left(1+\frac{r^2}{r_c^2}\right)^{-\frac{3}{2}\beta} \tag{A1}$$

out to the virial radius; and *(ii)* on average, the gas distribution is approximately isothermal and in hydrostatic equilibrium. In Coma[52], the central density is approximately $n_0 = (3.0\pm 0.6)\times 10^{-3}$ cm^{-3}, the core radius is $r_c = 343^{+22}_{-20}$ kpc, the index $\beta = 0.654^{+0.019}_{-0.021}$, and the (emission measure-weighted) temperature is $T = 8.38 \pm 0.34$ keV.

With the above assumptions, the region enclosing $\kappa = 200\kappa_{200}$ times the critical mass density ρ_c is characterized by

$$r_\kappa \simeq \left(\frac{9\beta T}{4\pi G \kappa \mu \rho_c}\right)^{1/2} \simeq 2.3 \kappa_{200}^{-1/2} \text{ Mpc} , \tag{A2}$$

$$M_\kappa \simeq \frac{3\beta T r_\kappa}{G\mu} \simeq 1.4\times 10^{15} \kappa_{200}^{-1/2} M_\odot , \tag{A3}$$

and

$$n_\kappa \equiv n(r_\kappa) \simeq 7.2\times 10^{-5} \kappa_{200} \text{ cm}^{-3} . \tag{A4}$$

We may now compute the accretion parameter,

$$\dot{m}_\kappa = \frac{4\pi r_\kappa^2 \mu n_\kappa v_\kappa}{f_b M_\kappa H} \simeq 1.4 \kappa_{200}^{1/2} , \tag{A5}$$

the inverse-Compton emissivity per unit shock area,

$$E^2 \frac{d^3N}{dt\,dA\,dE} \simeq \frac{3\xi_e f_b \dot{m} M_\kappa H k_B T}{16\pi r_\kappa^2 \mu \ln(\epsilon_{max}/m_e c^2)} \simeq 4.6 \times 10^{-8} \dot{m} \xi_{e,5} \kappa_{200}^{1/2} \text{ erg s}^{-1} \text{ cm}^{-2} \ , \tag{A6}$$

and the magnetic field at the shock,

$$B_\kappa = \sqrt{\xi_B 8\pi \frac{3}{2} n k_B T} \simeq 0.6 \kappa_{200}^{1/2} \xi_{B,1}^{1/2} \ \mu\text{G} \ . \tag{A7}$$

[1] A. Loeb and E. Waxman. Cosmic γ-ray background from structure formation in the intergalactic medium. *Nature (London)*, 405:156–158, May 2000.

[2] T. Totani and T. Kitayama. Forming Clusters of Galaxies as the Origin of Unidentified GEV Gamma-Ray Sources. *Astrophys. J.*, 545:572–577, December 2000.

[3] U. Keshet, E. Waxman, A. Loeb, V. Springel, and L. Hernquist. Gamma Rays from Intergalactic Shocks. *Astrophys. J.*, 585:128–150, March 2003.

[4] E. Waxman and A. Loeb. Fluctuations in the Radio Background from Intergalactic Synchrotron Emission. *ApJL*, 545:L11–L14, December 2000.

[5] F. Miniati. Intergalactic shock acceleration and the cosmic gamma-ray background. *MNRAS*, 337:199–208, November 2002.

[6] D. Kushnir and E. Waxman. Hard X-ray emission from accretion shocks around galaxy clusters. *Journal of Cosmology and Astro-Particle Physics*, 2:25–+, February 2010.

[7] U. Keshet, E. Waxman, and A. Loeb. Imprint of Intergalactic Shocks on the Radio Sky. *Astrophys. J.*, 617:281–302, December 2004.

[8] B. Kocsis, Z. Haiman, and Z. Frei. Can Virialization Shocks Be Detected around Galaxy Clusters through the Sunyaev-Zel'dovich Effect? *Astrophys. J.*, 623:632–649, April 2005.

[9] C. A. Scharf and R. Mukherjee. A Statistical Detection of Gamma-Ray Emission from Galaxy Clusters: Implications for the Gamma-Ray Background and Structure Formation. *Astrophys. J.*, 580:154–163, November 2002.

[10] P. Sreekumar, D. L. Bertsch, B. L. Dingus, J. A. Esposito, C. E. Fichtel, J. Fierro, R. C. Hartman, S. D. Hunter, G. Kanbach, D. A. Kniffen, Y. C. Lin, H. A. Mayer-Hasselwander, J. R. Mattox, P. F. Michelson, C. von Montigny, R. Mukherjee, P. L. Nolan, E. Schneid, D. J. Thompson, and T. D. Willis. EGRET Observations of the North Galactic Pole Region. *Astrophys. J.*, 464:628, June 1996.

[11] O. Reimer, M. Pohl, P. Sreekumar, and J. R. Mattox. EGRET Upper Limits on the High-Energy Gamma-Ray Emission of Galaxy Clusters. *Astrophys. J.*, 588:155–164, May 2003.

[12] M. Ackermann et al. GeV Gamma-ray Flux Upper Limits from Clusters of Galaxies. *ApJL*, 717:L71–L78, July 2010.

[13] The Veritas Collaboration with C. Pfrommer, A. P. T. Arlen, T. Aune, M. Beilicke, W. Benbow, A. Bouvier, J. H. Buckley, V. Bugaev, K. Byrum, A. Cannon, A. Cesarini, L. Ciupik, E. Collins-Hughes, M. P. Connolly, W. Cui, R. Dickherber, J. Dumm, A. Falcone, S. Federici, Q. Feng, J. P. Finley, G. Finnegan, L. Fortson, A. Furniss, N. Galante, D. Gall, S. Godambe, S. Griffin, J. Grube, G. Gyuk, J. Holder, H. Huan, G. Hughes, T. B. Humensky, A. Imran, P. Kaaret, N. Karlsson, M. Kertzman, Y. Khassen, D. Kieda, H. Krawczynski, F. Krennrich, K. Lee, A. S Madhavan, G. Maier, P. Majumdar, S. McArthur, A. McCann, P. Moriarty, R. Mukherjee, T. Nelson, A. O'Faoláin de Bhróithe, R. A. Ong, M. Orr, A. N. Otte, N. Park, J. S. Perkins, M. Pohl, H. Prokoph, J. Quinn, K. Ragan, L. C. Reyes, P. T. Reynolds, E. Roache, J. Ruppel, D. B. Saxon, M. Schroedter, G. H. Sembroski, C. Skole, A. W. Smith, I. Telezhinsky, G. Tešić, M. Theiling, S. Thibadeau, K. Tsurusaki, A. Varlotta, M. Vivier, S. P. Wakely, J. E. Ward, A. Weinstein, R. Welsing, D. A. Williams, and B. Zitzer. Constraints on Cosmic Rays, Magnetic Fields, and Dark Matter from Gamma-Ray Observations of the Coma Cluster of Galaxies with VERITAS and Fermi. *ArXiv e-prints*, August 2012.

[14] R. Gavazzi, C. Adami, F. Durret, J.-C. Cuillandre, O. Ilbert, A. Mazure, R. Pelló, and M. P. Ulmer. A weak lensing study of the Coma cluster. *A&A*, 498:L33–L36, May 2009.

[15] M. J. West, C. Jones, and W. Forman. Substructure: Clues to the Formation of Clusters of Galaxies. *ApJL*, 451:L5, September 1995.

[16] S. Brown and L. Rudnick. Diffuse Radio Emission in/around the Coma Cluster: Beyond Simple Accretion. *ArXiv e-prints*, September 2010.

[17] Planck Collaboration. Planck Intermediate Results. X. Physics of the hot gas in the Coma cluster. *ArXiv e-prints*, August 2012.

[18] M. K. Daniel. The VERITAS standard data analysis. In *International Cosmic Ray Conference*, volume 3 of *International Cosmic Ray Conference*, pages 1325–1328, 2008.

[19] R. Fusco-Femiano, M. Orlandini, M. Bonamente, and A. Lapi. Supermodel Analysis of the Hard X-ray Excess in the Coma Cluster. *Astrophys. J.*, 732:85, May 2011.

[20] R. Makiya, T. Totani, and K. Nakazawa. Suzaku Observation of Abell 1555 and Abell 1558: Searching for Non-thermal Emission from Large Scale Structure Formation. *ArXiv e-prints*, April 2012.

[21] E. Komatsu, K. M. Smith, J. Dunkley, C. L. Bennett, B. Gold, G. Hinshaw, N. Jarosik, D. Larson, M. R. Nolta, L. Page, D. N. Spergel, M. Halpern, R. S. Hill, A. Kogut, M. Limon, S. S. Meyer, N. Odegard, G. S. Tucker, J. L. Weiland, E. Wollack, and E. L. Wright. Seven-year Wilkinson Microwave Anisotropy Probe (WMAP) Observations: Cosmological Interpretation. *ApJS*, 192:18, February 2011.

[22] U. Keshet. Common origin for radio relics and halos: galaxy cluster-wide, homogeneous cosmic-ray distribution, and evolving magnetic fields. *ArXiv e-prints*, November 2010.

[23] T. A. Enßlin, R. Lieu, and P. L. Biermann. Non-thermal origin of the EUV and HEX excess emission of the Coma cluster - the nature of the energetic electrons. *A&A*, 344:409–420, April 1999.

[24] G. Brunetti, G. Setti, L. Feretti, and G. Giovannini. Particle reacceleration in the Coma cluster: radio properties and hard X-ray emission. *MNRAS*, 320:365–378, January 2001.

[25] B. Dennison. Formation of radio halos in clusters of galaxies from cosmic-ray protons. *ApJL*, 239:L93–L96, August 1980.

[26] D. Kushnir, B. Katz, and E. Waxman. Magnetic fields and cosmic rays in clusters of galaxies. *Journal of Cosmology and Astro-Particle Physics*, 9:24–+, September 2009.

[27] U. Keshet and A. Loeb. Using Radio Halos and Minihalos to Measure the Distributions of Magnetic Fields and Cosmic Rays in Galaxy Clusters. *Astrophys. J.*, 722:737–749, October 2010.

[28] F. Aharonian, A. G. Akhperjanian, G. Anton, U. Barres de Almeida, A. R. Bazer-Bachi, Y. Becherini, B. Behera, K. Bernlöhr, C. Boisson, A. Bochow, V. Borrel, E. Brion, J. Brucker, P. Brun, R. Bühler, T. Bulik, I. Büsching, T. Boutelier, P. M. Chadwick, A. Charbonnier, R. C. G. Chaves, A. Cheesebrough, L.-M. Chounet, A. C. Clapson, G. Coignet, M. Dalton, M. K. Daniel, I. D. Davids, B. Degrange, C. Deil, H. J. Dickinson, A. Djannati-Ataï, W. Domainko, L. O'C. Drury, F. Dubois, G. Dubus, J. Dyks, M. Dyrda, K. Egberts, D. Emmanoulopoulos, P. Espigat, C. Farnier, F. Feinstein, A. Fiasson, A. Förster, G. Fontaine, M. Füßling, S. Gabici, Y. A. Gallant, L. Gérard, B. Giebels, J. F. Glicenstein, B. Glück, P. Goret, D. Göhring, D. Hauser, M. Hauser, S. Heinz, G. Heinzelmann, G. Henri, G. Hermann, J. A. Hinton, A. Hoffmann, W. Hofmann, M. Holleran, S. Hoppe, D. Horns, S. Inoue, A. Jacholkowska, O. C. de Jager, C. Jahn, I. Jung, K. Katarzyński, U. Katz, S. Kaufmann, E. Kendziorra, M. Kerschhaggl, D. Khangulyan, B. Khélifi, D. Keogh, W. Kluźniak, T. Kneiske, N. Komin, K. Kosack, G. Lamanna, J.-P. Lenain, T. Lohse, V. Marandon, J. M. Martin, O. Martineau-Huynh, A. Marcowith, D. Maurin, T. J. L. McComb, M. C. Medina, R. Moderski, E. Moulin, M. Naumann-Godo, M. de Naurois, D. Nedbal, D. Nekrassov, J. Niemiec, S. J. Nolan, S. Ohm, J.-F. Olive, E. de Oña Wilhelmi, K. J. Orford, M. Ostrowski, M. Panter, M. Paz Arribas, G. Pedaletti, G. Pelletier, P.-O. Petrucci, S. Pita, G. Pühlhofer, M. Punch, A. Quirrenbach, B. C. Raubenheimer, M. Raue, S. M. Rayner, M. Renaud, O. Reimer, F. Rieger, J. Ripken, L. Rob, S. Rosier-Lees, G. Rowell, B. Rudak, C. B. Rulten, J. Ruppel, V. Sahakian, A. Santangelo, R. Schlickeiser, F. M. Schöck, R. Schröder, U. Schwanke, S. Schwarzburg, S. Schwemmer, A. Shalchi, M. Sikora, J. L. Skilton, H. Sol, D. Spanglfoer, Ł. Stawarz, R. Steenkamp, C. Stegmann, G. Superina, A. Szostek, P. H. Tam, J.-P. Tavernet, R. Terrier, O. Tibolla, M. Tluczykont, C. van Eldik, G. Vasileiadis, C. Venter, L. Venter, J. P. Vialle, P. Vincent, M. Vivier, H. J. Völk, F. Volpe, S. J. Wagner, M. Ward, A. A. Zdziarski, and A. Zech. Constraints on the multi-TeV particle population in the Coma galaxy cluster with HESS observations. *A&A*, 502:437–443, August 2009.

[29] U. Keshet, E. Waxman, and A. Loeb. The case for a low extragalactic gamma-ray background. *JCAP*, 4:6–+, April 2004.

[30] The map is cut into elliptical, $\Delta b = \theta = 0.2^\circ$ bins (Figure 1a), so $\Delta b \geq 0.8^\circ$ exceeds 2w at oblique angles.

[31] M. Ackermann, M. Ajello, W. B. Atwood, L. Baldini, J. Ballet, G. Barbiellini, D. Bastieri, K. Bechtol, R. Bellazzini, B. Berenji, R. D. Blandford, E. D. Bloom, E. Bonamente, A. W. Borgland, T. J. Brandt, J. Bregeon, M. Brigida, P. Bruel, R. Buehler, S. Buson, G. A. Caliandro, R. A. Cameron, P. A. Caraveo, E. Cavazzuti, C. Cecchi, E. Charles, A. Chekhtman, J. Chiang, S. Ciprini, R. Claus, J. Cohen-Tanugi, J. Conrad, S. Cutini, A. de Angelis, F. de Palma, C. D. Dermer, S. W. Digel, E. d. C. e. Silva, P. S. Drell, A. Drlica-Wagner, L. Falletti, C. Favuzzi, S. J. Fegan, E. C. Ferrara, W. B. Focke, P. Fortin, Y. Fukazawa, S. Funk, P. Fusco, D. Gaggero, F. Gargano, S. Germani, N. Giglietto, F. Giordano, M. Giroletti, T. Glanzman, G. Godfrey, J. E. Grove, S. Guiriec, M. Gustafsson, D. Hadasch, Y. Hanabata, A. K. Harding, M. Hayashida, E. Hays, D. Horan, X. Hou, R. E. Hughes, G. Jóhannesson, A. S. Johnson, R. P. Johnson, T. Kamae, H. Katagiri, J. Kataoka, J. Knödlseder, M. Kuss, J. Lande, L. Latronico, S.-H. Lee, M. Lemoine-Goumard, F. Longo, F. Loparco, B. Lott, M. N. Lovellette, P. Lubrano, M. N. Mazziotta, J. E. McEnery, P. F. Michelson, W. Mitthumsiri, T. Mizuno, C. Monte, M. E. Monzani, A. Morselli, I. V. Moskalenko, S. Murgia, M. Naumann-Godo, J. P. Norris, E. Nuss, T. Ohsugi, A. Okumura, N. Omodei, E. Orlando, J. F. Ormes, D. Paneque, J. H. Panetta, D. Parent, M. Pesce-Rollins, M. Pierbattista, F. Piron, G. Pivato, T. A. Porter, S. Rainò, R. Rando, M. Razzano, S. Razzaque, A. Reimer, O. Reimer, H. F.-W. Sadrozinski, C. Sgrò, E. J. Siskind, G. Spandre, P. Spinelli, A. W. Strong, D. J. Suson, H. Takahashi, T. Tanaka, J. G. Thayer, J. B. Thayer, D. J. Thompson, L. Tibaldo, M. Tinivella, D. F. Torres, G. Tosti, E. Troja, T. L. Usher, J. Vandenbroucke, V. Vasileiou, G. Vianello, V. Vitale, A. P. Waite, P. Wang, B. L. Winer, K. S. Wood, M. Wood, Z. Yang, M. Ziegler, and S. Zimmer. Fermi-LAT Observations of the Diffuse γ-Ray Emission: Implications for Cosmic Rays and the Interstellar Medium. *Astrophys. J.*, 750:3, May 2012.

[32] J. S. Perkins. VERITAS Observations of the Coma Cluster of Galaxies. In F. A. Aharonian, W. Hofmann, and F. Rieger, editors, *American Institute of Physics Conference Series*, volume 1085 of *American Institute of Physics Conference Series*, pages 569–572, December 2008.

[33] C. G. T. Haslam, C. J. Salter, H. Stoffel, and W. E. Wilson. A 408 MHz all-sky continuum survey. II - The atlas of contour maps. *A&AS*, 47:1, January 1982.

[34] W. Reich. A radio continuum survey of the northern sky at 1420 MHz. I. *A&AS*, 48:219–297, May 1982.

[35] D. P. Finkbeiner. A Full-Sky Hα Template for Microwave Foreground Prediction. *ApJS*, 146:407–415, June 2003.

[36] D. J. Schlegel, D. P. Finkbeiner, and M. Davis. Maps of Dust Infrared Emission for Use in Estimation of Reddening and Cosmic Microwave Background Radiation Foregrounds. *Astrophys. J.*, 500:525, June 1998.

[37] D. Lemze, R. Wagner, Y. Rephaeli, S. Sadeh, M. L. Norman, R. Barkana, T. Broadhurst, H. Ford, and M. Postman. Profiles of Dark Matter Velocity Anisotropy in Simulated Clusters. *Astrophys. J.*, 752:141, June 2012.

[38] B. Gold, N. Odegard, J. L. Weiland, R. S. Hill, A. Kogut, C. L. Bennett, G. Hinshaw, X. Chen, J. Dunkley, M. Halpern, N. Jarosik, E. Komatsu, D. Larson, M. Limon, S. S. Meyer, M. R. Nolta, L. Page, K. M. Smith, D. N. Spergel, G. S. Tucker, E. Wollack, and E. L. Wright. Seven-year Wilkinson Microwave Anisotropy Probe (WMAP) Observations: Galactic Foreground Emission. *ApJS*, 192:15, February 2011.

[39] G. Maier. Monte Carlo studies of the VERITAS array of Cherenkov telescopes. In *International Cosmic Ray Conference*, volume 3 of *International Cosmic Ray Conference*, pages 1413–1416, 2008.

[40] P. Blasi and S. Colafrancesco. Cosmic rays, radio halos and nonthermal X-ray emission in clusters of galaxies. *Astroparticle Physics*, 12:169–183, November 1999.

[41] V. Petrosian. On the Nonthermal Emission and Acceleration of Electrons in Coma and Other Clusters of Galaxies. *Astrophys. J.*, 557:560–572, August 2001.

[42] A. Bonafede, L. Feretti, M. Murgia, F. Govoni, G. Giovannini, D. Dallacasa, K. Dolag, and G. B. Taylor. The Coma cluster magnetic field from Faraday rotation measures. *A&A*, 513:A30+, April 2010.

[43] G. Brunetti, P. Blasi, O. Reimer, L. Rudnick, A. Bonafede, and S. Brown. Probing the origin of giant radio halos through radio and gamma-ray data : the case of the Coma cluster. *ArXiv e-prints*, July 2012.

[44] T. E. Clarke. Faraday Rotation Observations of Magnetic Fields in Galaxy Clusters. *Journal of Korean Astronomical Society*, 37:337–342, December 2004.

[45] M. Johnston-Hollitt. The Magnetic Field in A3667. In T. Reiprich, J. Kempner, & N. Soker, editor, *The Riddle of Cooling Flows in Galaxies and Clusters of galaxies*, pages 51–+, 2004.

[46] A. Bonafede, F. Govoni, L. Feretti, M. Murgia, G. Giovannini, and M. Brüggen. Fractional polarization as a probe of magnetic fields in the intra-cluster medium. *A&A*, 530:A24+, June 2011.

[47] D. Kushnir and E. Waxman. Nonthermal emission from clusters of galaxies. *Journal of Cosmology and Astro-Particle Physics*, 8:2–+, August 2009.

[48] B. De Lotto and Magic Collaboration. The MAGIC telescopes: performance, results and future perspectives. *Journal of Physics Conference Series*, 375(5):052021, July 2012.

[49] T. H. Burnett, M. Kerr, and M. Roth. Measurement of the Fermi-LAT Localization Performance. *ArXiv e-prints*, December 2009.

[50] A. Franceschini, G. Rodighiero, and M. Vaccari. Extragalactic optical-infrared background radiation, its time evolution and the cosmic photon-photon opacity. *A&A*, 487:837–852, September 2008.

[51] W. Benbow. The Status and Performance of H.E.S.S. In F. A. Aharonian, H. J. Völk, and D. Horns, editors, *High Energy Gamma-Ray Astronomy*, volume 745 of *American Institute of Physics Conference Series*, pages 611–616, February 2005.

[52] Y. Chen, T. H. Reiprich, H. Böhringer, Y. Ikebe, and Y.-Y. Zhang. Statistics of X-ray observables for the cooling-core and non-cooling core galaxy clusters. *A&A*, 466:805–812, May 2007.